REGULAR ARTICLE

blood advances

DNMT3A regulates murine megakaryocyte-biased hematopoietic stem cell fate decisions

Sarah M. Waldvogel,[1-4] Virginia Camacho,[5,6] Dandan Fan,[7] Anna G. Guzman,[1,2] Alejandra Garcia-Martell,[1,2] Elmira Khabusheva,[1,2] Jacey Rodriguez Pridgen,[1-3,8] Josephine De La Fuente,[1,2] Rachel Rau,[1,2,9] Ashlyn G. Laidman,[1,2,10] Maria N. Barrachina,[5,6] Estelle Carminita,[5,6] Justin A. Courson,[11,12] Michael R. Williamson,[2,13] Joanne I. Hsu,[1-3] Chun-Wei Chen,[1,2] Jaime Reyes,[1,2,8] Subhashree Pradhan,[1,11] Rolando E. Rumbaut,[11] Alan R. Burns,[14] Benjamin Deneen,[2,13] Jianzhong Su,[7] Kellie R. Machlus,[5,6] and Margaret A. Goodell[1,2,4,8]

[1]Department of Molecular and Cellular Biology, [2]Center for Cell and Gene Therapy, [3]Medical Scientist Training Program, and [4]Cancer and Cell Biology Graduate Program, Baylor College of Medicine, Houston, TX; [5]Vascular Biology Program, Boston Children's Hospital, Boston, MA; [6]Department of Surgery, Harvard Medical School, Boston, MA; [7]Oujiang Laboratory, Zhejiang Lab for Regenerative Medicine, Vision and Brain Health, Wenzhou, Zhejiang, China; [8]Genetics and Genomics Graduate Program, [9]Department of Pediatrics, and [10]Postbaccalaureate Research Education Program, Baylor College of Medicine, Houston, TX; [11]Center for Translational Research on Inflammatory Diseases, Michael E. DeBakey Veterans Affairs Medical Center, Houston, TX; [12]Department of Pulmonary, Critical Care and Sleep Medicine and [13]Department of Neurosurgery, Baylor College of Medicine, Houston, TX; and [14]Department of Vision Science, College of Optometry, University of Houston, Houston, TX

Key Points

- Megakaryocyte-biased HSCs deficient for DNMT3A exhibit delayed B cell reconstitution and unique regions of methylation loss.
- Reduced DNMT3A leads to lower methylation at megakaryocyte fate-specification loci and increases megakaryocyte numbers in the bone marrow.

Hematopoietic stem cells (HSCs) are defined by their capacity to regenerate all main components of peripheral blood, but individual HSCs exhibit a range of preferences for generating downstream cell types. Their propensities are thought to be epigenetically encoded, but few differential regulatory mechanisms have been identified. In this work, we explored the role of DNA methyltransferase 3A (DNMT3A) in the megakaryocyte-biased HSC population, which is thought to reside at the top of the hematopoietic hierarchy. We demonstrate that heterozygous loss of DNMT3A (*Dnmt3a*$^{+/-}$) in these megakaryocyte-biased HSCs has distinct consequences compared with the rest of the HSC pool. These megakaryocyte-biased HSCs become delayed in their lymphoid-repopulating ability but can ultimately regenerate all lineages. We further demonstrate that *Dnmt3a*$^{+/-}$ mice have increased numbers of megakaryocytes in the bone marrow. Analysis of DNA methylation differences between wild-type (WT) and *Dnmt3a*$^{+/-}$ HSC subsets, megakaryocyte-erythroid progenitors, and megakaryocytes revealed that DNA methylation is eroded in the mutants in a cell type–specific fashion. Although transcriptional differences between WT and *Dnmt3a*$^{+/-}$ megakaryocyte-biased HSCs are subtle, the pattern of DNA methylation loss in this HSC subset is almost completely different from that in non–megakaryocyte-biased HSCs. Together, our findings establish the role of epigenetic regulation in the fate of megakaryocyte-biased HSCs and their downstream progeny and suggest that the outcomes of *DNMT3A* loss might vary depending on the identity of the HSC that acquires the mutation.

Submitted 15 October 2024; accepted 14 February 2025; prepublished online on *Blood Advances* First Edition 6 March 2025. https://doi.org/10.1182/bloodadvances.2024015061.

Enzymatic methyl sequencing and bulk RNA sequencing data have been deposited in the Gene Expression Omnibus database (accession numbers GSE276903, GSE276901, GSE287995, and GSE287996).

Proteomics data are available in the ProteomeXchange Consortium via the Proteomics Identifications Database partner repository (data set identifier: PXD055265).

Further information, original data, resources, and reagents are available on reasonable request from the corresponding author, Margaret A. Goodell (goodell@bcm.edu).

The full-text version of this article contains a data supplement.

Introduction

Hematopoietic stem cells (HSCs) continuously replenish the differentiated cells of peripheral blood (PB). Recent studies established that HSCs are a heterogeneous population with different biases toward regeneration of specific lineages[1-7] (reviewed in Hass et al[8]). However, little is known about how these stem cell subtypes are differentially regulated. One well-defined subtype is biased toward the generation of megakaryocytes (Mks)/platelets.[9] These Mk-biased (Mk^{bi}) HSCs give rise to non-Mk^{bi} HSCs and all other cell types, but in transplantation, they preferentially reconstitute the platelet lineage.[9,10] They are conserved between mice and humans,[11] increase with age,[12] and contribute to increased thrombotic risk in aged individuals.[13]

Mk^{bi} HSCs bypass certain progenitor states in the pathway to Mk and platelet production.[14] This accelerated differentiation serves as a stress-response pathway to increase platelet counts in response to thrombocytopenia, inflammation, or infection.[15-17] Genetic tracing studies also indicate that the direct Mk differentiation pathway responds to niche-damaging stressors, such as chemotherapy, because it produces niche-supporting Mks to directly support HSCs.[18] Mk bias is thought to be epigenetically encoded in part through silencing of lymphoid upstream regulatory elements,[14] but specific mechanisms of Mk^{bi} HSC lineage fate programming remain to be defined.

DNA methyltransferase 3A (DNMT3A) is an epigenetic regulator of HSC lineage fate decisions. Loss of DNMT3A confers a self-renewal advantage upon HSCs and results in myeloid-biased differentiation,[19,20] ultimately leading to differentiation block after serial transplantation.[21] DNMT3A loss also leads to erosion at the edges of DNA methylation canyons, large regions of low methylation associated with stemness genes.[22] The resulting hypomethylation impairs the downregulation of HSC-identity genes and hinders progress toward differentiation. Additionally, the self-renewal advantage of *Dnmt3a*-mutant HSCs can be modulated by external factors, including inflammation.[23,24] However, despite its position as a key gatekeeper of HSC differentiation, the effects of DNMT3A loss have largely been examined in either bulk progenitors or the total long-term HSC (LT-HSC) population rather than in subtypes of lineage-biased or lineage-restricted LT-HSCs.

DNMT3A is one of the most commonly mutated genes in clonal hematopoiesis (CH), in which variant HSCs acquire a fitness advantage that leads to their clonal expansion over time,[25-27] which is associated with numerous adverse health outcomes.[25,26,28-32] Recent studies demonstrated that the epigenetic landscape primes hematopoietic cells for clonal dominance upon mutation acquisition, highlighting the importance of the cell's epigenetic identity before mutation.[33] However, it is unknown whether acquiring a *DNMT3A* mutation in a lineage-biased or lineage-restricted stem cell would have different effects on the outcomes of CH in the downstream progeny or whether loss of DNMT3A simply reprograms any LT-HSC, altering its properties or fate trajectory.

In this work, we explored the effect of DNMT3A loss on murine Mk^{bi} HSCs and found functional deficits specific to this subpopulation that also alter the function and molecular phenotypes of downstream progeny. Additionally, we implicate DNMT3A as a regulator of the Mk differentiation pathway.

Methods

Detailed versions of all methods are available in the supplemental Material.

Animal work

Mice were housed in Association for Assessment and Accreditation of Laboratory Animal Care-certified facilities at Baylor College of Medicine and approved by the Institutional Animal Care and Use Committee. The von Willebrand factor–green fluorescent protein (VWF-GFP) mouse[9] was crossed with *Dnmt3a*$^{+/-}$ mice[34] to obtain VWF-GFP/3aHET mice, maintained on a CD45.2 C57Bl/6 background. Littermates from multiple pooled litters were used in all experiments. $CD45.2^{+}$ HSCs were sorted and combined with $CD45.1^{+}$ whole bone marrow (WBM). Transplant donors were aged 6 to 16 weeks, and the ages of mice in all other experiments are stated in the text or figure legends. Recipients received a split dose of 11-Gy gamma irradiation and were retro-orbitally injected. Recipients with <0.5% CD45.2 engraftment were excluded from analysis.

Blood and bone marrow preparation for flow cytometry and fluorescence-activated cell sorting

WBM was collected from hindlimbs and pelvis. PB mononuclear cells were isolated using a heparin-dextran gradient and red blood cell lysis. Antibodies and markers are listed in the supplement. Samples were analyzed and sorted on a BD LSR II or FACSAria.

Mk ex vivo differentiation and proplatelet formation

Mouse bone marrow was cultured with thrombopoietin and recombinant hirudin for 3 days. Mks were purified using a bovine serum albumin gradient. Proplatelet formation was visualized using time-lapse microscopy for 24 hours on a Leica TCS SP8 and quantified.[35]

Bone marrow immunofluorescence

Mouse femurs were fixed in 4% paraformaldehyde, decalcified (0.2-M EDTA), and cryoprotected with sucrose. Frozen sections of 14 μm were obtained on the Cryostar Nx70 and stained with a-CD41 ± a-laminin. Imaging was performed on the Keyence BZ-X800 or Zeiss LSM900. Mks were manually counted across the length of the femur. Mk size was analyzed in ImageJ or Photoshop.

Platelet isolation and analysis

Blood was collected into acid citrate dextrose, and washed platelets were isolated by differential centrifugation and quantified on a complete blood count machine (Balio OV-360). For RNA sequencing (RNAseq), platelets were purified with a-Ter119 and a-CD45. For transmission electron microscopy, platelets[36] were fixed and suspended in agarose, then treated with 1% tannic acid, followed by 1% osmium tetroxide (aqueous), dehydrated in an acetone series, and embedded in Embed-812 resin. Sections of 100 nm were imaged on a Tecnai G2 Spirit BioTWIN EM. Platelet aggregation assays were performed[37] after treatment with indicated thrombin concentrations and staining with a-Ter119, a-CD41, and a-CD62P at room temperature for 20 minutes. For proteomics, the platelet pellet was lysed and digested, and the tryptic peptides were subjected to liquid chromatography with tandem mass spectrometry analysis using a nano-LC 1200 system coupled to Orbitrap Exploris 480.

Sequencing

One to 10 ng of DNA was used for the NEBNext Enzymatic Methyl-Seq kit. More than 200 ng of RNA was used for Tru-Seq messenger RNA kit. The Takara Bio SMARTer Stranded Total RNA kit (v3, Pico Mammalian Input) was used for low input RNA-seq. Data analysis is described in the supplemental Material.

Hemorrhagic stroke model

Striatal hemorrhage was induced by stereotactic injection of 250 nL of 0.1 U/μL type IV collagenase. Twenty-four hours later, total hemoglobin within each hemisphere (hemorrhage and non-hemorrhage) was determined at 560 nm after combining brain homogenate with Drabkin reagent.[38]

Statistical analysis

Statistics were performed using GraphPad Prism and R studio. Results that reached statistical significance are indicated in figures as follows: *$P \leq .05$; **$P \leq .01$; ***$P \leq .001$; ****$P \leq .0001$.

Results

Reduced DNMT3A results in LT-HSC skewing, but fewer are Mk^{bi}

We began by characterizing the effect of heterozygous DNMT3A loss using competitive WBM transplantation. To track platelets, we crossed germ line *Dnmt3a*$^{+/-}$ mice (referred to throughout as 3aHET) with the VWF-GFP reporter mouse line, in which GFP is expressed under the VWF promoter, resulting in GFP-labeled platelets, Mks, and Mk^{bi} HSCs.[9] We mixed WBM from VWF-GFP 3aHET donors with that from CD45.1 wild-type (WT) donors at a 20:80 ratio and transplanted it into lethally irradiated CD45.1 recipients (Figure 1A). We monitored donor chimerism as the percentage of CD45.2$^+$ leukocytes or GFP$^+$ platelets. Over the course of 20 weeks, there were no significant differences in PB donor chimerism (supplemental Figure 1A), donor chimerism in the B cell, T cell, or myeloid compartments in the bone marrow (supplemental Figure 1B), LT-HSC donor chimerism (supplemental Figure 1C), or the percentage of CD45.2$^+$GFP$^+$ (Mk^{bi}) LT-HSCs (supplemental Figure 1D).

Because serial transplantation has been shown to exacerbate DNMT3A phenotypes,[19,21] we pooled WBM from primary recipients and retransplanted it into secondary recipients (Figure 1A). There was no significant difference in overall PB donor chimerism (Figure 1B) or donor chimerism within B cells, T cells, myeloid cells, or platelets (Figure 1C). However, within the CD45.2$^+$ progenitors (Lineage^{neg}, Sca1$^+$ cKit$^+$ [LSK]; see the supplemental Methods for definitions), the 3aHET group demonstrated significant skewing toward the LT-HSC compartment at the expense of the more differentiated multipotent progenitor-3/4 (MPP3/4) population[39] (Figure 1D-E). These progenitor-level changes did not translate into differences in the composition of differentiated bone marrow (Figure 1F). However, within the test LT-HSC population, the 3aHET cells exhibited a lower percentage of GFP$^+$ (Mk^{bi}) HSCs (Figure 1G). When we quantified Mks based on GFP and CD41 staining in cryosectioned femurs of transplant recipients (supplemental Figure 1E), we found no difference in the percentage of GFP$^+$ Mks (supplemental Figure 1F), Mk area, (supplemental Figure 1G), or the total number of Mks (supplemental Figure 1H). Additionally, there was no difference in platelet or total white blood cell counts (supplemental Figure 1I). Together, these data show that DNMT3A loss promotes progenitor skewing toward LT-HSCs but may have differential effects on Mk^{bi} vs non-Mk^{bi} HSCs.

3aHET Mk^{bi} HSCs are poorly transplantable and exhibit delayed B cell reconstitution

To clarify the differential effects of DNMT3A loss on different subpopulations of HSCs, we transplanted GFP$^+$ (Mk^{bi}) or GFP$^-$ (non-Mk^{bi}) LT-HSCs from either WT or 3aHET VWF-GFP donors (Figure 2A; supplemental Figure 2A). Unexpectedly, the 3aHET Mk^{bi} HSCs failed to engraft in over half of the recipient mice (Figure 2B). In contrast, WT Mk^{bi} HSCs, WT non-Mk^{bi} HSCs, and 3aHET non-Mk^{bi} HSCs exhibited no engraftment deficiencies. These results were consistent across male and female sorted donor pools, as well as across multiple transplants performed months apart.

In engrafted recipient mice, the contribution of 3aHET Mk^{bi} HSCs to overall PB donor chimerism was significantly delayed (supplemental Figure 2B). The 3aHET Mk^{bi} condition exhibited delayed ability to reconstitute the B cell lineage compared with WT Mk^{bi} HSCs but robustly generated the myeloid/platelet lineages (Figure 2C). 3aHET Mk^{bi} HSCs were also delayed in their T cell reconstitution capacity but not more so than WT Mk^{bi} HSCs. Although it is well established that Mk^{bi} HSCs exhibit platelet/myeloid skewing,[9,10,14] this phenomenon was more pronounced in 3aHET Mk^{bi} HSCs (Figure 2C). The 3aHET Mk^{bi} HSC condition also exhibited high absolute platelet counts by complete blood count at the 24-week end point (supplemental Figure 2C). At this time, there were no differences in LSK or LT-HSC donor chimerism in Mk^{bi} recipients, suggesting that the delayed lymphoid reconstitution in the 3aHET Mk^{bi} condition was not due to a failure of HSCs to seed the bone marrow but rather due to functional deficits and delayed differentiation (supplemental Figure 2D).

We also assessed the composition of the progenitor compartment. Skewing toward LT-HSCs at the expense of MPP3/4 within the CD45.2$^+$ LSK compartment occurred in recipients of 3aHET Mk^{bi} HSCs (Figure 2D). These results are consistent with findings in the competitive WBM transplant setting, demonstrating the distinct reliance of Mk^{bi} HSCs on DNMT3A. Mk^{bi} HSCs of both genotypes were better at reconstituting Mk^{bi} HSCs in recipients than their non-Mk^{bi} counterparts (Figure 2E; supplemental Figure 2E).

Finally, we examined Mk production. Although donor chimerism within the Mk populations was similar (supplemental Figure 2F), the total number of Mks per area was higher in the 3aHET non-Mk^{bi} condition than the WT non-Mk^{bi} or WT Mk^{bi} conditions (supplemental Figure 2G). The fact that the 3aHET Mk^{bi} HSC condition produces more absolute platelets (supplemental Figure 2C) without having a larger number of Mks suggests that Mks derived from these cells are more productive. In total, these data indicate that Mk^{bi} 3aHET HSCs exhibit engraftment deficiencies, delayed B cell reconstitution, and platelet bias without gross Mk expansion.

HET Mk^{bi} HSCs display enhanced transcriptional signatures of low output and Mk bias

To better understand the altered hematopoietic reconstitution properties of Mk^{bi} 3aHET HSCs, we analyzed previously generated

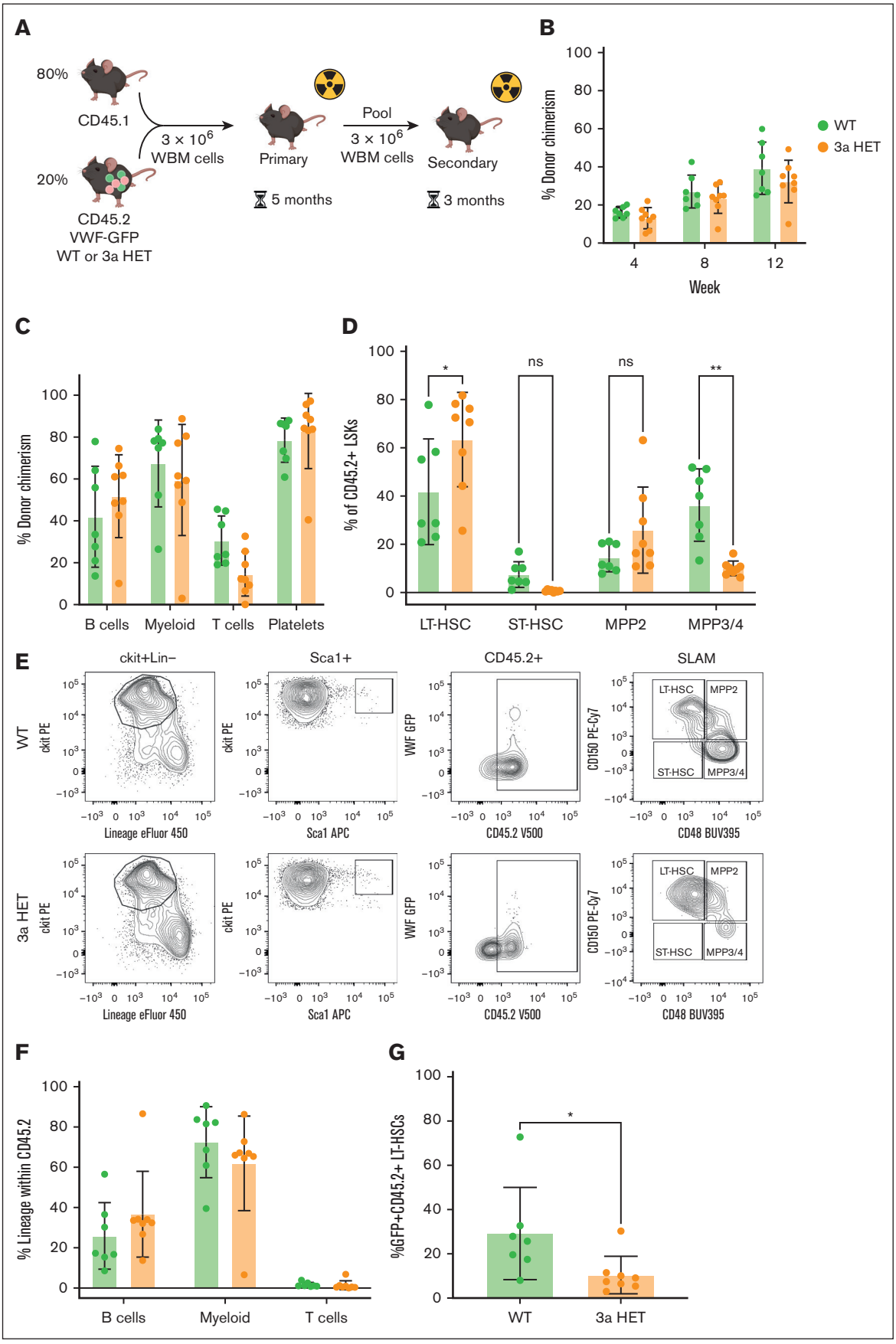
A
80%
CD45.1
20%
CD45.2
VWF-GFP
WT or 3a HET
3 × 10^6
WBM cells
Primary
5 months
Pool
3 × 10^6
WBM cells
Secondary
3 months
B
% Donor chimerism
Week
WT
3a HET
C
% Donor chimerism
B cells
Myeloid
T cells
Platelets
D
% of CD45.2+ LSKs
LT-HSC
ST-HSC
MPP2
MPP3/4
ns
**
E
ckit+Lin−
Sca1+
CD45.2+
SLAM
WT
3a HET
ckit PE
Lineage eFluor 450
Sca1 APC
VWF GFP
CD45.2 V500
CD150 PE-Cy7
CD48 BUV395
F
% Lineage within CD45.2
G
%GFP+CD45.2+ LT-HSCs

Figure 1.

single-cell RNAseq data from WT or 3aHET LSK cells 10 months after WBM transplantation.[40] We identified Mk^{bi} HSCs as cells expressing *Vwf* transcripts (supplemental Figure 3A-B). As expected within the LSK compartment, these were mostly confined to the population annotated as LT-HSCs (Figure 3A; supplemental Figure 3A,C). Differential gene expression analysis between WT and 3aHET *Vwf*$^{+}$ LT-HSCs suggested higher expression of genes that suppress cell motility in 3aHET HSCs, a feature of quiescence[41] (Figure 3B; supplemental Table 1). Supportive of these findings, the *Vwf*$^{+}$ 3aHET cells more closely matched an Mk-biased (Figure 3C) and low-output HSC signature (Figure 3D).[5] These findings are consistent with our previous work demonstrating that *Dnmt3a*-knockout HSCs have difficulty exiting G0 and express lower levels of Ki67 in response to stimulation[42] but indicate that this phenotype may be more prominent in mutant *Vwf*$^{+}$ HSCs.

However, we noticed that the number of differentially expressed genes unique to *Vwf*$^{+}$ 3aHET vs WT and not shared with *Vwf*$^{-}$ 3aHET vs WT was relatively small (supplemental Figure 3D-I), although these small differences led to very different pathway enrichment annotations between the 2 comparisons (Figure 3B; supplemental Figure 3J). Area under the curve scores for Mk-biased, low-output, and high-output signatures (supplemental Figure 3K-M), as well as the expression of key HSC marker genes (supplemental Figure 3C), gave us confidence that our *Vwf* expression cutoff was biologically meaningful. However, we recognized that the population might slightly differ from the one we sorted in our transplants. Therefore, we performed bulk RNAseq on sorted WT and 3aHET Mk^{bi} and non-Mk^{bi} HSCs. High expression of *Vwf* and *Slamf1* (CD150) and low expression of *Flt3* in the Mk^{bi} HSC samples validated the quality of our sorting strategy (Figure 4A). We compared Mk^{bi} to non-Mk^{bi} HSCs within the WT and 3aHET genotypes and then looked for differentially expressed genes that were unique to each comparison (Figure 4B-C; supplemental Table 2). Pathways related to cell motility and chemokine response were upregulated uniquely in Mk^{bi} 3aHET HSCs (Figure 4B), similar to the single-cell data. The bulk RNAseq data also revealed an enrichment of platelet-derived growth factor signaling unique to Mk^{bi} 3aHET HSCs (Figure 4B). Very few genes were uniquely downregulated in Mk^{bi} 3aHET HSCs (Figure 4C). Overall, transcriptional HSC identity in the steady state was influenced much more significantly by intrinsic HSC bias than by *Dnmt3a* genotype.

Germ line 3aHET animals display phenotypic abnormalities at the Mk level

We wondered whether the observed changes were unique to the transplant context or whether phenotypic differences might be present in germ line 3aHET bone marrow. We sectioned mouse femurs and found that the number of Mks per area of bone marrow was significantly increased in 3aHETs (Figure 5A). Furthermore, 3aHET Mk morphology appeared qualitatively different from WT Mks, with abnormal borders that were similar in appearance to those described in mice fed a high-fat diet,[35] suggesting a possible change in membrane morphology (Figure 5B). However, unlike in the transplant context, there were only very minor differences in LSK composition, with slightly less contribution from 3aHET MPP3/4 (Figure 5C). In young animals, there were no differences in the proportion of Mk^{bi} LT-HSCs (Figure 5D). Although in aged WT animals, we observed the expected[11-13] increase in Mk^{bi} HSCs, this increase was significantly muted in 3aHET animals (Figure 5D). We assessed a different stressor by administering 5-fluorouracil (5-FU) or phosphate-buffered saline to WT and 3aHET mice and examined their LT-HSC compartment 7 days after treatment (Figure 5E). Although the Mk^{bi} HSC percentage increased in both genotypes after 5-FU treatment compared with phosphate-buffered saline, there was no difference between the genotypes, suggesting that 3aHET Mk^{bi} HSCs are equally capable of surviving and responding to this short-term stress as WT Mk^{bi} HSCs.

We next investigated the function of 3aHET platelets. We did not observe any differences in ex vivo activation or aggregation (supplemental Figure 4A-C). They had no visible or quantifiable (supplemental Figure 4D-E) morphological abnormalities when spread on fibrinogen-coated coverslips. Moreover, by transmission electron microscopy, we did not observe significant morphological differences (supplemental Figure 4F). Finally, in Mks differentiated ex vivo, there was no difference in proplatelet area or the percent of Mks forming proplatelets (supplemental Figure 4G-H). However, proteomics analysis and RNAseq of platelets from 3aHET mice indicated numerous molecular changes. Notably, in proteomics data, several structural components, including numerous members of the α-tubulin family, were downregulated in 3aHET compared with WT (Figure 5F). In RNAseq data, metabolic genes were downregulated, as well as components of the coagulation and

Figure 1. Reduced DNMT3A results in LT-HSC skewing, but fewer are Mk^{bi}. (A) Experimental design. WBM (3×10^6 cells) was transplanted into lethally irradiated CD45.1 recipients. The transplanted WBM was composed of 80% CD45.1 cells and 20% test cells, either VWF-GFP 3a WT or VWF-GFP *Dnmt3a*$^{+/-}$ ("3aHET"). Test cells were CD45.2. After 5 months, bone marrow from all primary recipients of the same sex and genotype was pooled and transplanted into lethally irradiated CD45.1 secondary recipients. Blood was sampled every 4 weeks for a total of 12 weeks. Primary transplant included 15 mice per genotype, including both male and female mice; secondary transplant included 7 WT and 8 3aHET female mice. (B) PB donor chimerism in WT and 3aHET secondary transplant recipients over 12 weeks (n = 7 WT and 8 3aHET female mice). Two-way analysis of variance (ANOVA) with Šídák multiple comparisons test. All comparisons not significant (ns) with a *P* value of >.05. Data are represented as the mean ± standard deviation (SD). (C) PB donor chimerism within the B cell, myeloid, T cell, and platelet lineages in WT and 3aHET secondary transplant recipients at 12 weeks (n = 7 WT and 8 3aHET female mice). Two-way ANOVA with Šídák multiple comparisons test. All comparisons ns with a *P* value of >.05. Data are represented as the mean ± SD. (D) Quantification of the percentage of test CD45.2^{+} LSK cells composed of LT-HSCs and MPP3/4 in WT and 3aHET secondary transplant recipients. Flow cytometry counts within each of the 4 groups were summed, and the percentage was calculated from the total (n = 7 WT and 8 3aHET female mice). Two-way ANOVA with Šídák multiple comparisons test. *$P \leq .05$; **$P \leq .01$. Data are represented as the mean ± SD. (E) Flow cytometry gating strategy for the data represented in panel D. Lineage-depleted bone marrow cells were gated as ckit^{+} Lineage−negative Sca1^{+} CD45.2^{+} and then divided into LT-HSCs (CD150^{hi}CD48^{lo}), ST-HSCs (CD150^{lo}CD48^{lo}), MPP2 (CD150^{hi}CD48^{hi}), and MPP3/4 (CD150^{lo}CD48^{hi}). (F) WBM donor chimerism within the B cell, myeloid, and T cell lineages of WT and 3aHET secondary transplant recipients at 12 weeks (n = 7 WT and 8 3aHET female mice). Two-way ANOVA with Šídák multiple comparisons test. All comparisons ns with a *P* value of >.05. Data are represented as the mean ± SD. (G) The percentage of test CD45.2^{+} LT-HSCs that are Mk^{bi} in the WT and 3aHET secondary transplant recipients. Mann-Whitney test; *$P \leq .05$ (n = 7 WT and 8 3aHET female mice). Data are represented as the mean ± SD. ST-HSC, short-term HSC; MPP3/4, multipotent progenitor-3/4.

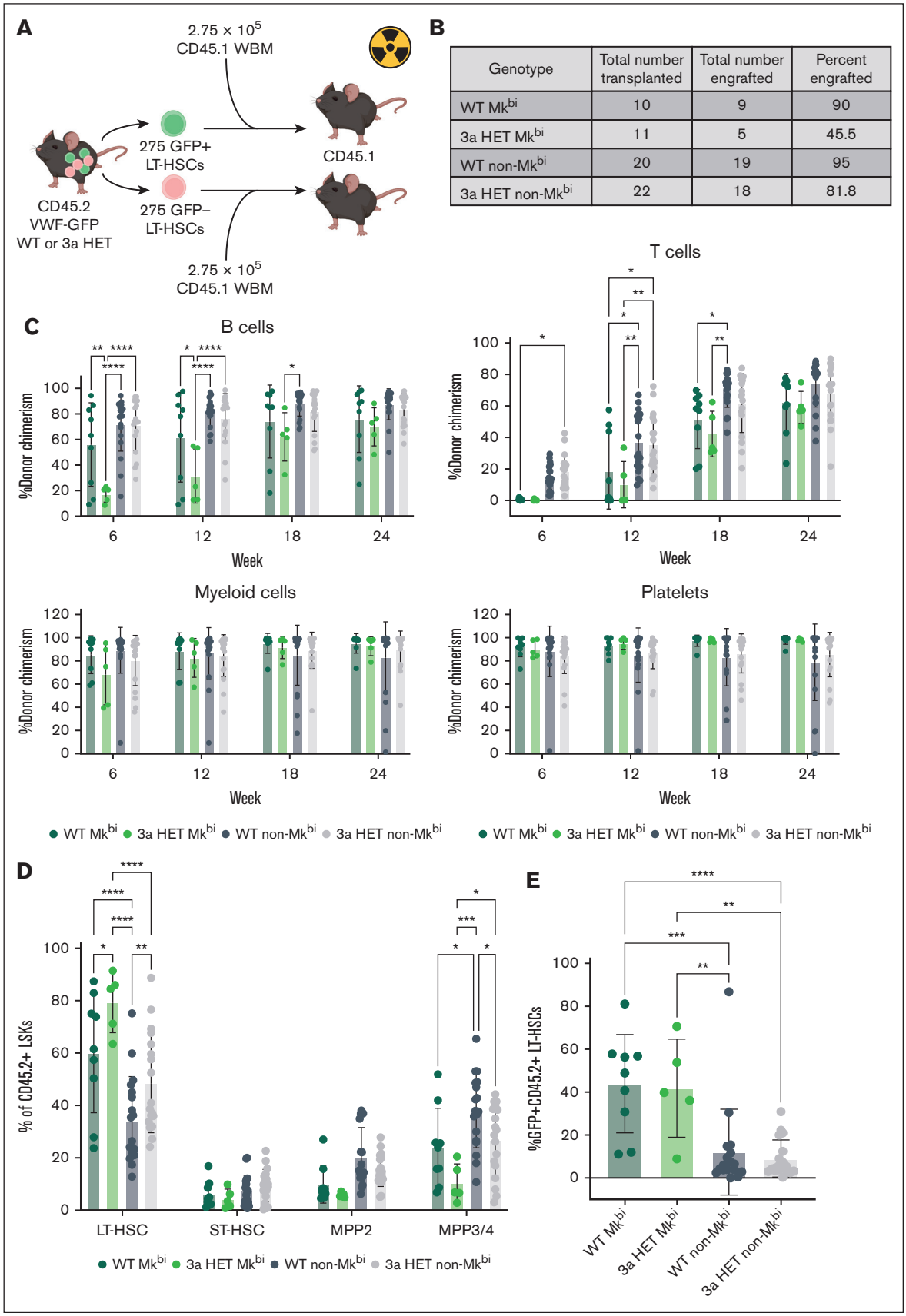

Genotype	Total number transplanted	Total number engrafted	Percent engrafted
WT Mk^{bi}	10	9	90
3a HET Mk^{bi}	11	5	45.5
WT non-Mk^{bi}	20	19	95
3a HET non-Mk^{bi}	22	18	81.8

Figure 2. 3aHET Mk^{bi} HSCs are poorly transplantable and exhibit delayed B cell reconstitution. (A) Experimental design. Mk^{bi} (GFP^{+}) and non-Mk^{bi} (GFP^{-}) LT-HSCs were sorted from VWF-GFP 3a WT or VWF-GFP 3aHET CD45.2 donors. A total of 275 LT-HSCs (GFP^{+} or GFP^{-}) were mixed with 275 000 supporting CD45.1 WBM cells and

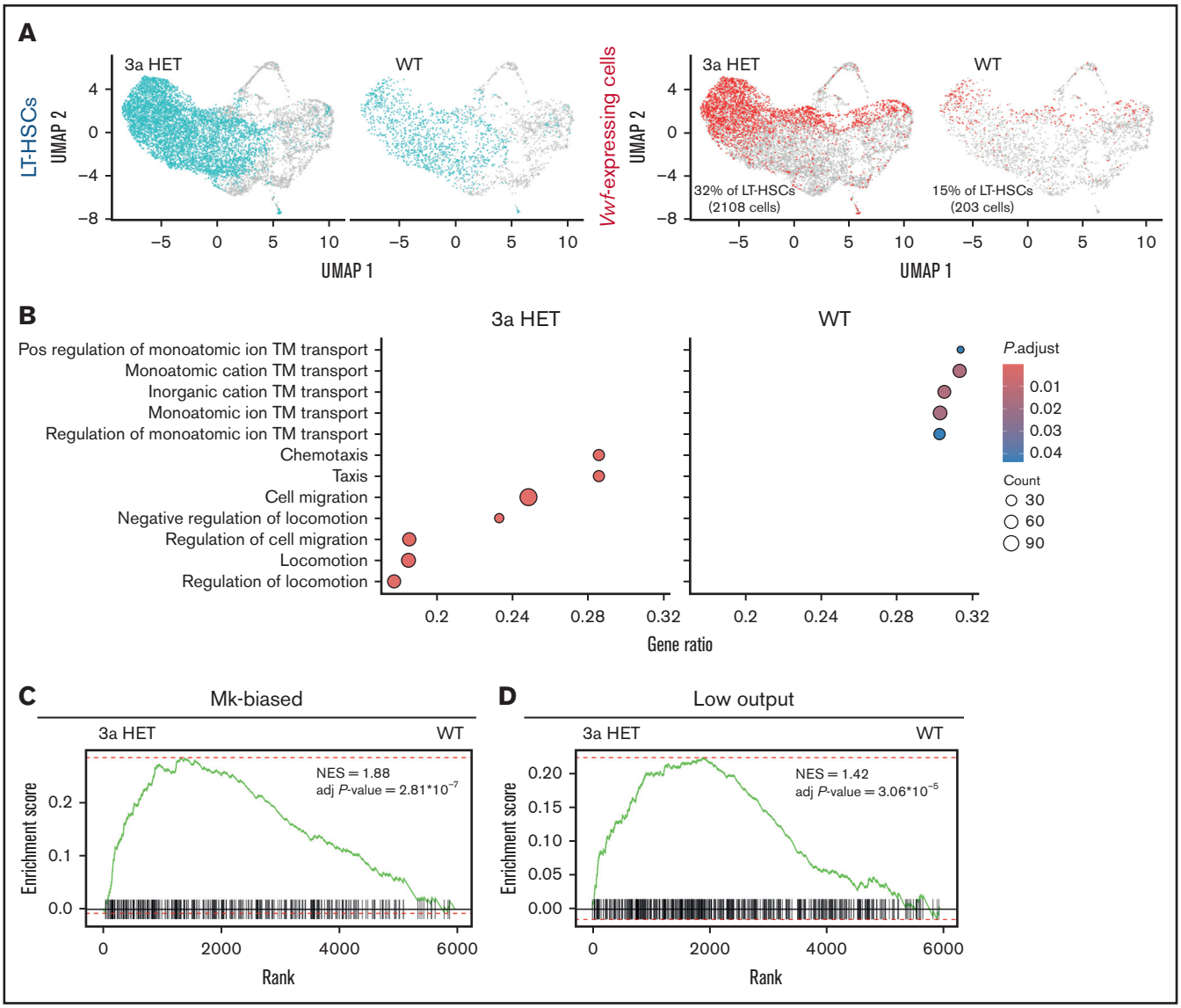

Figure 3. 3aHET Mk^{bi} HSCs display enhanced transcriptional signatures of low output and Mk-bias. (A) Uniform Manifold Approximation and Projection plot of cell type distribution for WT and 3aHET single-cell RNAseq data sets from 2 pooled mice per genotype 10 months after WBM transplant (data set from Reyes et al[40]). CD45.2$^+$ LSKs were sorted for sequencing. Immunological Genome Project reference cell type LT-HSCs, SC.LT34F (CD34$^-$FLK2$^-$ LT-HSCs; CD34$^-$Flk2$^-$Lin$^-$c-kit$^+$Sca1$^+$) are highlighted in blue, and cells expressing >0 *Vwf* transcripts are highlighted in red. (B) Gene set enrichment analysis interaction terms from differentially expressed genes between 3aHET and WT *Vwf*$^+$ LT-HSCs. An adjusted *P* value of < .05 was set as the threshold for significantly related genes, displaying the top 7 significant pathways. The gene list was generated by ranking the log2FC in decreasing order. (C) Fast gene set enrichment analysis plot of differentially expressed genes in 3aHET and WT *Vwf*$^+$ HSCs compared with the Mk-biased output HSC signature.[5] A total of 1000 gene permutations were used to calculate statistical significance, and an adjusted *P* value of <.05 was set for statistical significance of the gene sets. (D) Fast gene set enrichment analysis plot of differentially expressed genes in 3aHET and WT *Vwf*+ HSCs compared with the low-output HSC signature.[5] One-thousand gene permutations were used to calculate statistical significance, and an adjusted *P* value of <.05 was set for statistical significance of the gene sets. adj, adjusted; NES, normalized enrichment score; Pos, positive; TM, transmembrane.

Figure 2 (continued) transplanted into lethally irradiated CD45.1 recipients. Blood was collected from the recipients every 6 weeks for 24 weeks. Cells from male and female donors were pooled separately and transplanted into male recipients. The data shown are from a combination of 2 transplants performed at separate times with separate donor pools. (B) The number of mice that were transplanted with HSCs and the outcome for each group combined from 2 separate transplants. The total number engrafted, and the percent engrafted indicate mice that survived to 6 weeks after transplant and exhibited >0.5% donor chimerism in the PB or bone marrow. A single mouse in the Mk^{bi} 3aHET group survived long term with <0.5% donor chimerism. All other mice that failed to engraft died within ~3 weeks after transplant. (C) The percent donor chimerism in the PB B cells, T cells, myeloid cells, and platelets from 6 to 24 weeks after transplant in the HSC transplant recipients. Two-way ANOVA with Šídák multiple comparisons test. *$P \leq .05$; **$P \leq .01$; ***$P \leq .001$; ****$P \leq .0001$. Data are represented the mean ± SD. (D) The composition of the CD45.2$^+$ LSK compartment with regard to the indicated stem and progenitor cells as gated in Figure 1E. Two-way ANOVA with Šídák multiple comparisons test. *$P \leq .05$; **$P \leq .01$; ***$P \leq .001$; ****$P \leq .0001$. Data are represented as the mean ± SD. (E) The percent of Mk^{bi} CD45.2$^+$ LT-HSCs in Mk^{bi} vs non-Mk^{bi} transplant recipients. One-way ANOVA with Tukey multiple comparisons test. *$P \leq .05$; **$P \leq .01$; ***$P \leq .001$; ****$P \leq .0001$. Data are represented as the mean ± SD. ST-HSC, short-term HSC; MPP3/4, multipotent progenitor-3/4.

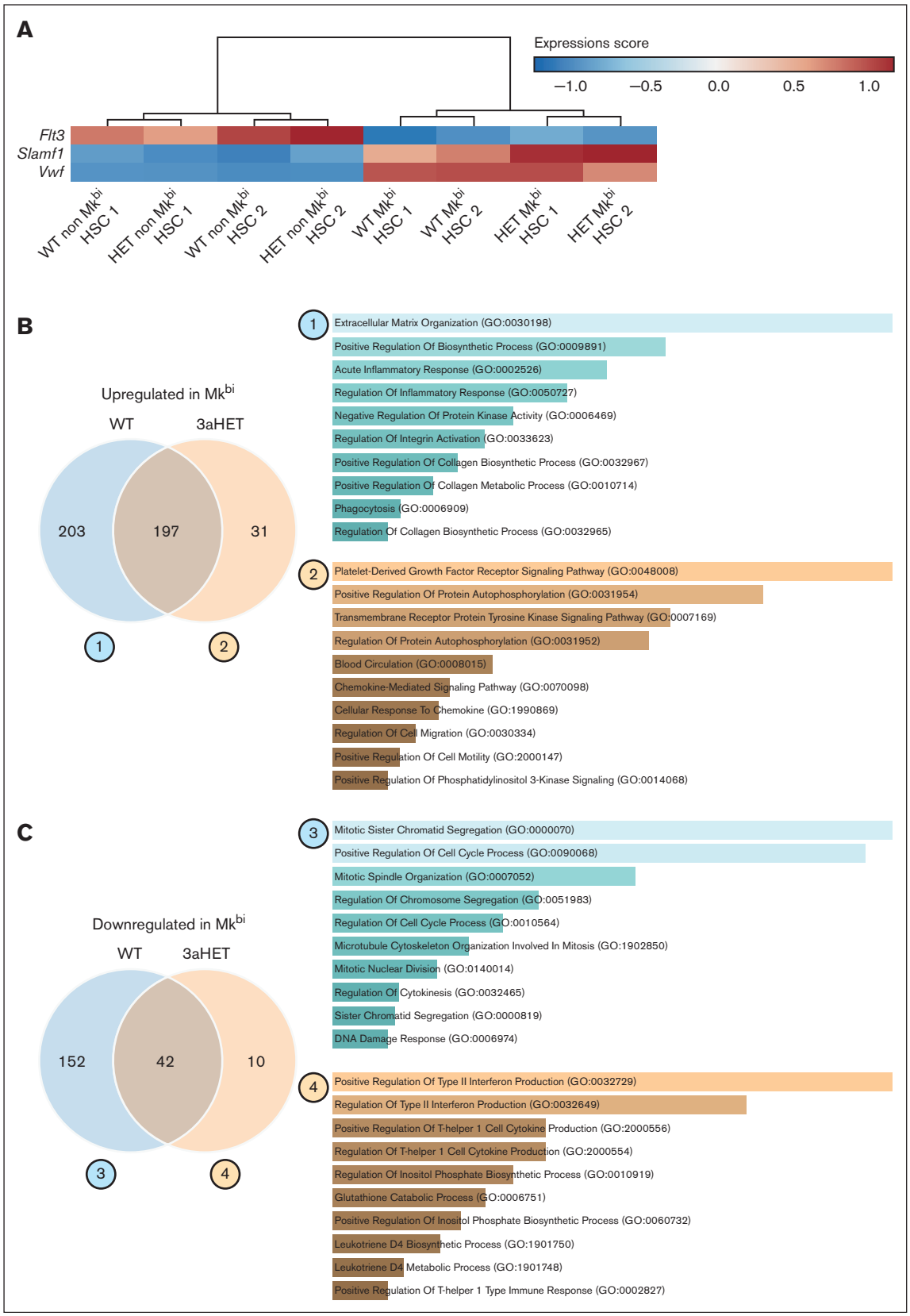

Figure 4. Transcriptional cell identity is determined more by intrinsic HSC bias than genotype. (A) Heat map showing the expression levels of key marker genes from bulk RNAseq of Mk^{bi} and non-Mk^{bi} HSCs from pooled WT and 3aHET mice. Mk^{bi} and non-Mk^{bi} HSCs were sorted from a pool of male and female mice for each genotype (n = 3-4

complement cascades (Figure 5G). Because patients with DNMT3A-mutant CH are at increased risk of hemorrhagic stroke,[28] we transplanted WT and 3aHET WBM into irradiated WT recipients (to avoid potential effects of *Dnmt3a* loss in the vasculature of germ line 3aHETs) and induced hemorrhagic strokes via collagenase injection. However, there were no differences in intracerebral hematoma volume between mice with WT or 3aHET bone marrow (supplemental Figure 4I). Thus, although 3aHET mice have more Mks, the structure and function of 3aHET platelets are grossly normal in mice and in ex vivo activation assays.

3aHET Mk^{bi} and non-Mk^{bi} HSCs, MEPs, and Mks exhibit unique hypomethylation patterns

We sought to determine how de novo DNA methylation might be altered in the 3aHET context in Mk^{bi} and non-Mk^{bi} HSCs, as well as in downstream cells during Mk lineage specification. We sorted Mk^{bi} and non-Mk^{bi} HSCs and Mk-erythroid progenitors (MEPs) from WT and 3aHET mice and generated Mks via ex vivo culture for whole-genome enzymatic methyl sequencing (supplemental Tables 3 and 4).

Both Mk^{bi} and non-Mk^{bi} 3aHET HSCs exhibited >1000 differentially methylated regions (DMRs) compared with their WT counterparts, and most were areas of decreased methylation (hypoDMRs), as expected given the heterozygous loss of *Dnmt3a* (Figure 6A). However, these DMRs were mostly unique to each HSC type, with only 2 shared areas of increased methylation (hyperDMRs) and 38 shared hypoDMRs between Mk^{bi} and non-Mk^{bi} 3aHET HSCs compared with WT (Figure 6A). This finding suggests that *Dnmt3a* loss has almost completely different effects on the methylation landscape of the 2 types of LT-HSCs, emphasizing the importance of considering them separately rather than in bulk. Downstream, 3aHET MEPs mostly exhibited hypoDMRs compared with WT MEPs, whereas 3aHET Mks had regions of both significantly increased and significantly decreased methylation (Figure 6B). There is also limited overlap between genes that exhibited hypomethylation or hypermethylation in 3aHET MEPs and 3aHET Mks compared with their WT counterparts (supplemental Figure 5A), further supporting the cell type specificity of DNMT3A-mediated methylation.

We first focused on DMRs in Mk^{bi} and non-Mk^{bi} HSCs. Integrative clustering revealed groups of non-Mk^{bi}–specific hyperDMRs and hypoDMRs, Mk^{bi}-specific hyperDMRs and hypoDMRs, and common hypoDMRs (Figure 6C). We explored the functional annotations associated with these clusters (Figure 6D). We were most interested in DMRs specific to 3aHET Mk^{bi} HSCs, because these cells were functionally deficient in transplant. 3aHET Mk^{bi}-specific hyperDMRs involved adenosine triphosphate and glycoprotein metabolism, whereas 3aHET Mk^{bi}-specific hypoDMRs involved cell adhesion, secretion, and several signaling pathways (platelet-derived growth factor and Rap1) (Figure 6D), some of which were also identified in the matched bulk RNAseq data (Figure 4B).

We also wondered how methylation changes in 3aHET Mk^{bi} HSCs might compare with those in 3aHET Mks (Figure 6E). Common hypoDMRs between 3aHET Mk^{bi} HSCs and Mks involved oxidative stress response and cytoskeletal organization. Mk^{bi}-specific hypoDMRs involved negative regulation of cell motility, whereas Mk-specific hypoDMRs were nearly all related to various cell signaling pathways (Figure 6F).

We next compared 3aHET and WT MEPs. The functional annotations associated with 3aHET MEP hypoDMRs were striking and involved cell junction and cell projection organization, calcium signaling, and phosphorylation (supplemental Figure 5B). The relatively small number of hypermethylated DMRs showed less significance and apparent functional relevance (supplemental Figure 5C). Finally, we compared 3aHET and WT Mks. 3aHET Mk hypoDMRs involved secretion, cell migration, and proliferation (supplemental Figure 5D), whereas 3aHET Mk hyperDMRs included cell junction and cell projection organization (supplemental Figure 5E).

To better understand the differences common to both MEPs and Mks in the 3aHET context, we performed integrative clustering of DMRs (supplemental Figure 5F) and focused on cluster 5, which represents hypoDMRs that are shared between 3aHET MEPs and Mks (supplemental Figure 5F, red box). Cluster 5 genes are involved in platelet/Mk development and platelet production (supplemental Figure 5G). Some genes implicated in this pathway, such as *Gata3*, are hypomethylated specifically in 3aHET Mk^{bi} HSCs but not in 3aHET non-Mk^{bi} HSCs. Others, such as *Jmjd1c*, are hypomethylated specifically in 3aHET non-Mk^{bi} HSCs but not in 3aHET Mk^{bi} HSCs. In total, our methylation sequencing results depict a landscape of epigenetic dysregulation in 3aHET mice that is unique to each cell type and differs vastly even within the LT-HSC compartment.

Discussion

Here, we demonstrate that heterozygous loss of *Dnmt3a* differentially affects LT-HSC subtypes. It has been previously reported that Mk^{bi} HSCs are more quiescent than their non-Mk^{bi} counterparts.[5,14] However, this has largely been reported to enhance their transplantability.[5] With loss of just 1 allele of *Dnmt3a*, 3aHET Mk^{bi} HSCs appear to have delayed hematopoietic reconstitution. Furthermore, we found that 3aHET *Vwf*-expressing LT-HSCs corresponded to an Mk-biased and low-output signature[5] more closely than their WT counterparts. This is further evidence that the Mk^{bi} state of LT-HSCs is epigenetically encoded,[14] and DNMT3A is a key regulator of LT-HSC identity.

It is well known that complete ablation of DNMT3A enhances stem cell self-renewal at the expense of differentiation.[19,21] Even though in our study, the HSCs retain 1 intact *Dnmt3a* allele, we can observe the essence of this phenotype; however, it is mostly confined to the specific Mk^{bi} subset of HSCs rather than the bulk

Figure 4 (continued) mice per pool; aged 10-12 months). Expression type = transcript per million, samples ordered by Euclidean hierarchical clustering, transformed by row-wise z score. (B) Venn diagram showing the genes upregulated in Mk^{bi} HSCs compared with non-Mk^{bi} HSCs. A total of 203 genes are unique to the WT Mk^{bi} vs WT non-Mk^{bi} comparison, 31 genes are unique to the 3aHET Mk^{bi} vs 3aHET non-Mk^{bi} comparison, and 197 genes are upregulated in both. The top Gene Ontology-Biological Process (GO-BP) terms for genes uniquely upregulated in WT (blue, 1) and uniquely upregulated in 3aHET (orange, 2) are shown ranked by *P* value. (C) Venn diagram showing the genes downregulated in Mk^{bi} HSCs compared with non-Mk^{bi} HSCs. A total of 152 genes are unique to the WT Mk^{bi} vs WT non-Mk^{bi} comparison, 10 genes are unique to the 3aHET Mk^{bi} vs 3aHET non-Mk^{bi} comparison, and 42 genes are downregulated in both. The top GO-BP terms for genes uniquely downregulated in WT (blue, 3) and uniquely downregulated in 3aHET (orange, 4) are shown ranked by *P* value.

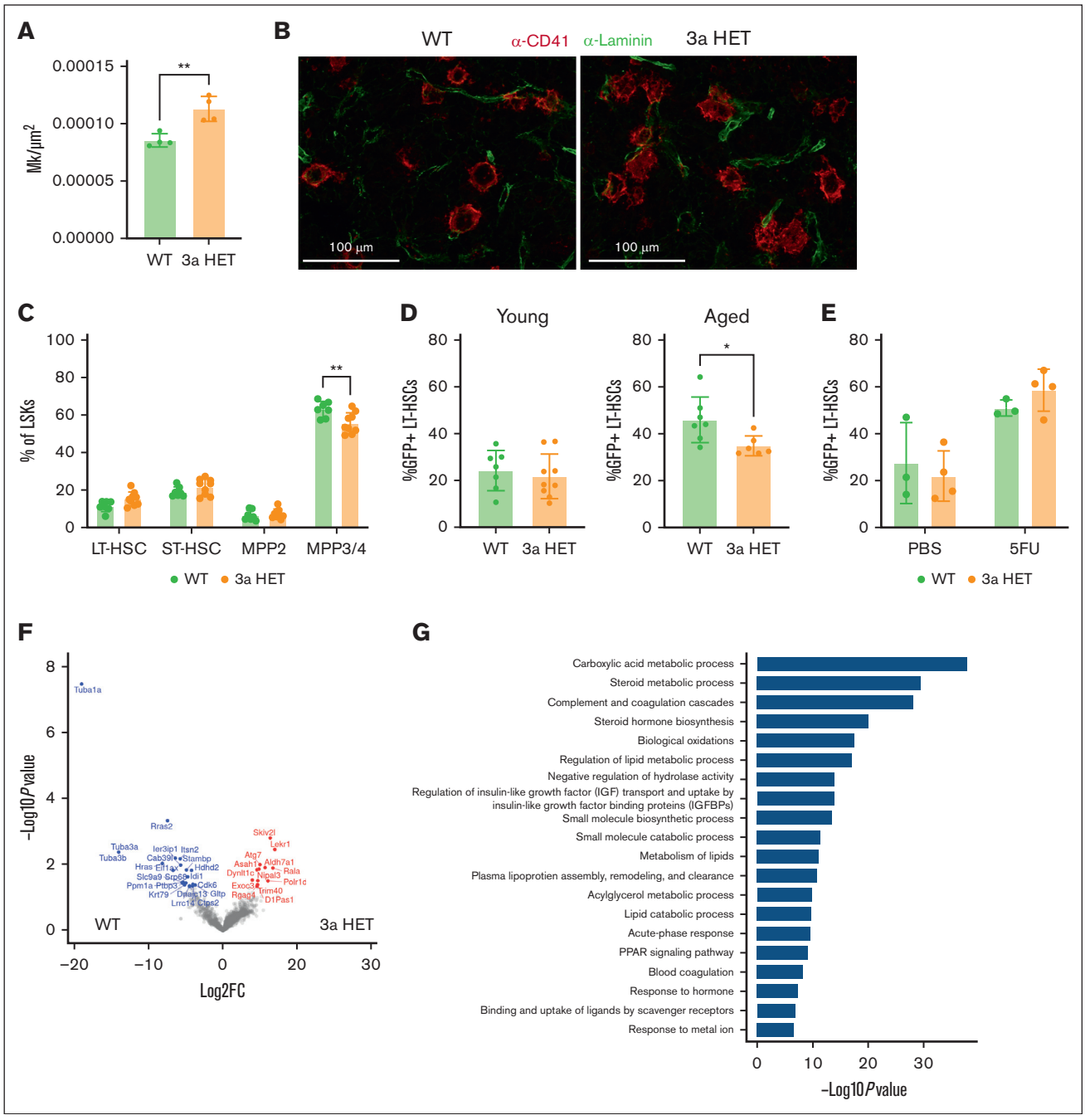

Figure 5. Germ line 3aHET animals display phenotypic abnormalities at the Mk level. (A) Quantification of Mks per µm in WT vs 3aHET mice via immunofluorescence imaging of bone marrow sections from mouse femurs (n = 4 female mice per group; aged 4 months); and the entire length of 1 femur was imaged. $^{**}P \leq .01$. Data are represented as the mean ± SD. (B) Representative images of WT and 3aHET Mks from frozen femur sections (red = α-CD41, AF647; green = α-Laminin, AF488; scale bar = 100 mm). Imaged on the Zeiss LSM900 confocal microscope with the Plan-Apo 20× objective and displayed as an orthogonal projection of the stack using the Zen Blue software. The channels were overlaid, the images were cropped, and scale bars were applied in ImageJ. (C) Quantification of the composition of the LSK compartment in WT vs 3aHET germ line animals (n = 7 WT and 9 3aHET, both male and female mice; aged 2-4 months). Two-way ANOVA with Šídák multiple comparisons test. $^{**}P \leq .01$. Data are represented as the mean ± SD. (D) The percent of GFP^+ HSCs in germ line 3aHET animals. Young animals included 7 WT and 9 3aHET, both male and female mice; aged 2 to 4 months. Unpaired *t* test. $P > .05$ (ns). Data are represented as the mean ± SD. Old animals included 7 WT and 6 3aHET, both male and female mice; aged 9 to 12 months. Unpaired *t* test. $P > .05$ (ns). Data are represented as the mean ± SD. (E) The percent of GFP^+ HSCs in germ line 3aHET animals 7 days after treatment with PBS or 5FU (n = 3 WT mice and 4 3aHET mice per group, both male and female mice; aged 2-10 months; ages matched between groups). Two-way ANOVA with Šídák multiple comparisons test. $P > .05$ (ns). Data are represented as the mean ± SD. (F) Volcano plot showing the differentially expressed proteins, as determined by mass spectrometry, between WT (−log2FC) and 3aHET (+log2FC) platelets (n = 4 per group, including 2 males and 2 females; aged 2 months). (G) Gene ontology analysis of platelet RNAseq showing pathways downregulated in the 3aHET samples (n = 4 males per group; aged 3 months). ns, not significant; PBS, phosphate-buffered saline; ST-HSC, short term HSC.

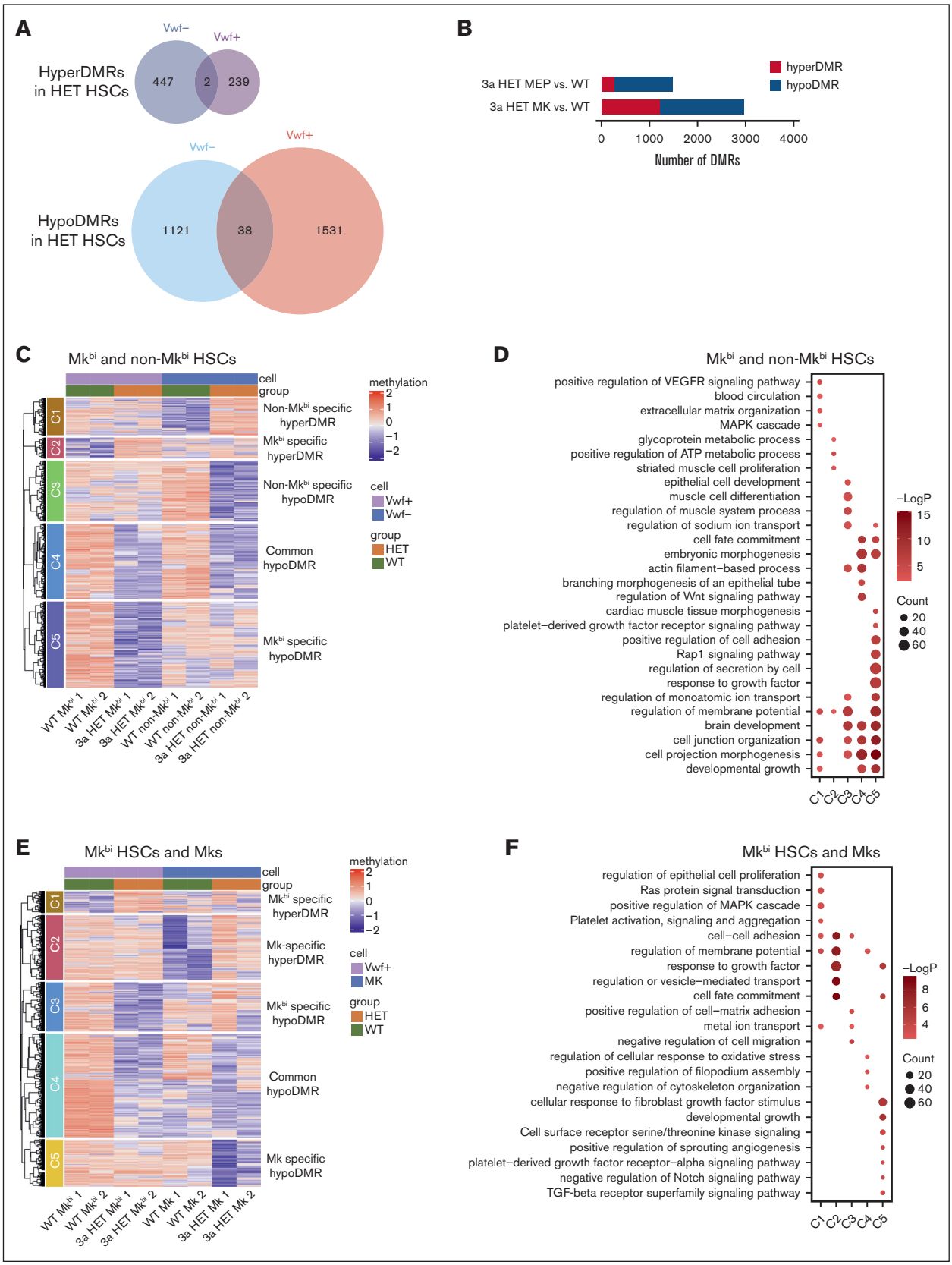

Figure 6. 3aHET Mk^{bi} and non-Mk^{bi} HSCs, MEPs, and Mks exhibit unique hypomethylation patterns. (A) Shared and unique regions of decreased methylation (hypo-) and increased methylation (hyper-) in 3aHET compared with WT from Mk^{bi} and non-Mk^{bi} HSCs. Mk^{bi} and non-Mk^{bi} HSCs were sorted from a pool of male and female mice for

population. The LT-HSC skewing was most pronounced in Mk^{bi} 3aHET HSCs when purified cells were transplanted, although it occurred to a lesser degree in non-Mk^{bi} 3aHET HSCs. The delayed B cell production is unique to 3aHET Mk^{bi} HSCs. Our work, therefore, demonstrates that DNMT3A loss affects different subsets of the LT-HSC population to different degrees and may differentially regulate pluripotency exit based on the HSC's intrinsic identity. The classic "myeloid bias" of HSCs lacking DNMT3A may be a hallmark of 3aHET Mk^{bi} HSCs rather than non-Mk^{bi} LT-HSCs. It is notable that when bulk WBM was transplanted, 3aHET Mk^{bi} HSCs were depleted, and this depletion compared with WT also occurred with aging but not with 5-FU treatment. 3aHET Mk^{bi} HSCs thus appear intolerant of long-term stressors but capable of persisting under short-term duress.

It is also striking that many recipients of 3aHET Mk^{bi} HSCs did not survive, despite receiving an amount of supporting WBM cells that should have supported hematopoiesis. We suggest that 3aHET Mk^{bi} HSCs may exhibit suppressive effects on the competitor WBM but fail to differentiate efficiently, hindering the regeneration of remaining marrow and blood components necessary for rescue from lethal irradiation. The potential for interaction between 3aHET Mk^{bi} HSCs and competitor bone marrow is an intriguing possibility that warrants further follow-up. Additionally, single HSC transplants or barcoding experiments might further elucidate whether the observed phenotypes result from altered composition or bias within the *Vwf*$^{+}$ HSC pool, which is known to still exhibit somewhat heterogeneous potential,[43] or whether they are caused by uniform intrinsic functional deficits within the Mk^{bi} HSC compartment.

In addition to the effects on 3aHET Mk^{bi} HSC function, we report more subtle changes downstream in Mks and platelets, with more Mks but no substantial platelet phenotypes. It is possible that the in vivo functions of mutant platelets might be subtly altered; however, due to the extremely high platelet counts in mouse blood (1000×10^9/L to 1500×10^9/L in mice compared with 150×10^9/L to 400×10^9/L in humans)[44] and a number of physiologic peculiarities, mice can be difficult models for detecting subtle thrombosis and hemostasis phenotypes.[45] Additionally, metabolic defects might not be apparent in culture conditions with serum or might only be present in cells derived from aged animals.

One of our most striking findings is that there are many more DMRs than differentially expressed genes when comparing WT and 3aHET HSC subsets. 3aHET HSCs function relatively normally in the steady state, and thus, we are unsurprised by the relatively minor transcriptional changes. However, as our functional data demonstrate, the substantial methylation changes that are present at the HSC level likely impair its ability to mount appropriate responses to transplant and aging, resulting in altered differentiation trajectories. Additionally, Mk^{bi} and non-Mk^{bi} HSCs exhibit almost completely different DMRs in 3aHET compared with WT, emphasizing the differential epigenetic effects exerted by DNMT3A loss in these 2 cell types.

DNMT3A likely plays a specific role in the Mk/platelet lineage, because we show methylation changes at key loci in the normal transition from progenitors to Mks, which are altered in 3aHET mice. De novo DNA methylation has previously been implicated in Mk specification using methyl-binding domain sequencing,[46] which showed that differentiation of Mks compared with the erythroid lineage involved a massive reorganization of the methylome. However, the genome-wide Mk methylation landscape has not been previously examined, and no enzymes have been shown to be responsible for its reorganization. The regions that failed to become methylated in 3aHET MEPs and 3aHET Mks relative to WT were grouped into relevant functional categories, such as hemostasis, Mk development, and platelet production. It is interesting to consider whether Mks derived from direct and indirect differentiation pathways might exhibit different methylation patterns and whether they might more closely resemble the methylation patterns of one subset of HSCs over another.

In the germ line context, we were unable to distinguish between the output of Mk^{bi} HSCs and non-Mk^{bi} HSCs, because this requires lineage tracing.[13,18,47] Therefore, it is unclear which population contributes to the increased number of Mks per area of bone marrow in germ line 3aHET mice or whether other environmental factors, such as increased inflammatory signaling,[34,40] contribute to the output differences. However, in the transplant setting, it is clearly the non-Mk^{bi} 3aHET HSCs that produce elevated numbers of Mks per area of bone marrow rather than the Mk^{bi} 3aHET HSCs (supplemental Figure 2G). This finding may be consistent with the idea that the traditional differentiation pathway, from the HSC through a cascade of progenitors, is responsible for producing immune Mks that respond to inflammatory stress.[18]

Overall, our results suggest that DNMT3A loss might have pleiotropic effects depending on the type of stem cell that acquires the mutation. Notably, DNMT3A loss higher in the HSC hierarchy appears to cause the most substantial changes in self-renewal and differentiation potential. This finding may have implications for CH, suggesting a relevance for the type of HSC carrying the mutation. Indeed, the order of *DNMT3A* vs additional mutations can affect outcomes.[33,48] We speculate that our work might explain the frequent occurrence of DNMT3A mutations in essential thrombocythemia, a myeloproliferative neoplasm characterized by excessive platelet production,[48] in which Mk^{bi} HSCs are thought to be the source of the malignancy.[11,49] These data reinforce the concept that DNMT3A is important for promoting normal hematopoietic differentiation into all lineages in a rapid fashion and underscore the exquisite dosage sensitivity of HSCs to the presence of DNMT3A.

Acknowledgments

The authors thank Kwangwon Lee and Antrix Jain for their assistance with the sample preparation and data analysis. The authors are grateful to Sten Eirik Jacobsen for sharing the VWF-GFP reporter mouse line. Figure schematics were created with BioRender.com.

Figure 6 (continued) each genotype (n = 3-4 mice per pool; aged 10-12 months). DNA was isolated from the same samples used for bulk RNAseq in Figure 4. (B) Total number of DMRs in 3aHET MEPs and Mks compared with WT (n = 2 female mice per group; aged 6 months). (C) Integrative clustering of DMRs from Mk^{bi} and non-Mk^{bi} HSCs in 3aHET compared with WT. (D) Functional enrichment of the clusters from panel C. (E) Integrative clustering of DMRs from Mk^{bi} HSCs and Mks in 3aHET compared with WT. (F) Functional enrichment of the clusters from panel E. C1, cluster 1; HET, 3aHET; TGF, transforming growth factor; VEGFR, vascular endothelial growth factor receptor.

This project was supported by the Cytometry and Cell Sorting Core at Baylor College of Medicine (supported by Cancer Prevention and Research Institute of Texas grant CPRIT-RP180672, National Intitutes of Health [NIH]/National Cancer Institute [NCI] grant CA125123, and NIH grant RR024574) and the assistance of Joel M. Sederstrom. The Mass Spectrometry Proteomics Core is supported by NIH/NCI grant CA125123, Cancer Prevention and Research Institute of Texas grant RP210227, and NIH grant S10 OD026804. The Genomics and RNA Profiling Core is supported by NIH/National Institute of Diabetes and Digestive and Kidney Diseases (NIDDKD) grant NIDDK-DK56338 and NIH/NCI grant CA125123, NIH/National Institute of Environment and Health Sciences grant NIEHS-5P30ES030285-03, Cancer Prevention and Research Institute of Texas grant 1S10OD02346901.

The authors gratefully acknowledge the following funding sources: the Eunice Kennedy Shriver National Institute of Child Health and Human Development (F30HD111129; S.M.W.), the Robert and Janice McNair Foundation MD/PhD Scholars program (S.M.W.), and Baylor Research Advocates for Student Scientists (S.M.W.). The Goodell Lab is supported by NIH/NCI grants CA183252, CA265748, and CA237291, NIDDKD grant DK092883, and NIH/National Institute of Aging grant AG036695. The study was supported in part by Merit Review Award I01 BX002551 from the Department of Veterans Affairs Biomedical Laboratory Research & Development Service (R.E.R.). J.A.C. was supported by the NIH/National Heart, Lung, and Blood Institute (NHLBI) T32 Training program HL139425 and VA CDA-2 IK2BX006462. A.R.B. is supported by NIH grant P30 EY007551. The Machlus Lab is supported by NIDDKD grant R01DK139341; K.R.M., NHLBI grants R01HL151494 (K.R.M.) and K99HL175037 (M.N.B.), the American Society of Hematology (ASH) Scholar Award (V.C.), and American Heart Association grant 24IPA1274573 (K.R.M.). The Deneen Lab is supported by NIH/National Institute of Neurological Disorders and Strokes grant R35-NS132230 (B.D.) and American Heart Association grant AHA-23POST1019413 (M.R.W.). A.G.L. is supported via the Baylor College of Medicine PREP Scholars program NIH/National Institute of General Medical Sciences grant R25GM069234.

The contents presented herein do not represent the views of the US Department of Veterans Affairs or the US Government.

Authorship

Contribution: S.M.W., K.R.M., and M.A.G. contributed to conceptualization; S.M.W., V.C., A.G.G., A.G.-M., R.R., A.G.L., J.A.C., M.R.W., J.I.H., S.P., E.K., C.-W.C., and J.R.P. conducted investigations; S.M.W., D.F., J.D.L.F., J.R., M.N.B., E.C., J.A.C., E.K., and J.R.P. performed formal analysis; S.M.W. and M.A.G. wrote the original draft of the manuscript; S.M.W., V.C., M.A.G., K.R.M., and J.R.P. reviewed and edited the manuscript; and R.E.R., A.R.B., M.A.G., K.R.M., B.D., and J.S. provided supervision.

Conflict-of-interest disclosure: The authors declare no competing financial interests.

ORCID profiles: S.M.W., 0000-0002-3657-1951; J.R.P., 0000-0002-4117-7166; R.R., 0000-0003-4096-6603; A.G.L., 0009-0001-6944-0245; E.C., 0000-0002-8544-4879; J.A.C., 0000-0002-1036-097X; M.R.W., 0000-0002-8049-4463; C.-W.C., 0000-0001-6761-3002; J.R., 0000-0001-7895-2472; R.E.R., 0000-0002-8486-1013; K.R.M., 0000-0002-2155-1050; M.A.G., 0000-0003-1111-2932.

Correspondence: Margaret A. Goodell, Baylor College of Medicine, 1 Baylor Plaza, Alkek N1030, Houston, TX 77030; email: goodell@bcm.edu.

References

1. Dykstra B, Kent D, Bowie M, et al. Long-term propagation of distinct hematopoietic differentiation programs in vivo. *Cell Stem Cell*. 2007;1(2):218-229.
2. Challen GA, Boles NC, Chambers SM, Goodell MA. Distinct hematopoietic stem cell subtypes are differentially regulated by TGF-beta1. *Cell Stem Cell*. 2010;6(3):265-278.
3. Benz C, Copley MR, Kent DG, et al. Hematopoietic stem cell subtypes expand differentially during development and display distinct lymphopoietic programs. *Cell Stem Cell*. 2012;10(3):273-283.
4. Copley MR, Beer PA, Eaves CJ. Hematopoietic stem cell heterogeneity takes center stage. *Cell Stem Cell*. 2012;10(6):690-697.
5. Rodriguez-Fraticelli AE, Weinreb C, Wang SW, et al. Single-cell lineage tracing unveils a role for TCF15 in haematopoiesis. *Nature*. 2020;583(7817):585-589.
6. Weinreb C, Rodriguez-Fraticelli A, Camargo FD, Klein AM. Lineage tracing on transcriptional landscapes links state to fate during differentiation. *Science*. 2020;367(6479):eaaw3381.
7. Li L, Bowling S, McGeary SE, et al. A mouse model with high clonal barcode diversity for joint lineage, transcriptomic, and epigenomic profiling in single cells. *Cell*. 2023;186(23):5183-5199.e22.
8. Haas S, Trumpp A, Milsom MD. Causes and consequences of hematopoietic stem cell heterogeneity. *Cell Stem Cell*. 2018;22(5):627-638.
9. Sanjuan-Pla A, Macaulay IC, Jensen CT, et al. Platelet-biased stem cells reside at the apex of the haematopoietic stem-cell hierarchy. *Nature*. 2013;502(7470):232-236.
10. Carrelha J, Meng Y, Kettyle LM, et al. Hierarchically related lineage-restricted fates of multipotent haematopoietic stem cells. *Nature*. 2018;554(7690):106-111.
11. Aksöz M, Gafencu GA, Stoilova B, et al. Hematopoietic stem cell heterogeneity and age-associated platelet bias are evolutionarily conserved. *Sci Immunol*. 2024;9(98):eadk3469.
12. Grover A, Sanjuan-Pla A, Thongjuea S, et al. Single-cell RNA sequencing reveals molecular and functional platelet bias of aged haematopoietic stem cells. *Nat Commun*. 2016;7:11075.

13. Poscablo DM, Worthington AK, Smith-Berdan S, et al. An age-progressive platelet differentiation path from hematopoietic stem cells causes exacerbated thrombosis. *Cell*. 2024;187(12):3090-3107.e21.
14. Meng Y, Carrelha J, Drissen R, et al. Epigenetic programming defines haematopoietic stem cell fate restriction. *Nat Cell Biol*. 2023;25(6):812-822.
15. Morodomi Y, Kanaji S, Sullivan BM, et al. Inflammatory platelet production stimulated by tyrosyl-tRNA synthetase mimicking viral infection. *Proc Natl Acad Sci U S A*. 2022;119(48):e2212659119.
16. Haas S, Hansson J, Klimmeck D, et al. Inflammation-induced emergency megakaryopoiesis driven by hematopoietic stem cell-like megakaryocyte progenitors. *Cell Stem Cell*. 2015;17(4):422-434.
17. Frisch BJ, Hoffman CM, Latchney SE, et al. Aged marrow macrophages expand platelet-biased hematopoietic stem cells via interleukin1B. *JCI Insight*. 2019;5(10):e124213.
18. Li JJ, Liu J, Li YE, et al. Differentiation route determines the functional outputs of adult megakaryopoiesis. *Immunity*. 2024;57(3):478-494.e6.
19. Challen GA, Sun D, Jeong M, et al. Dnmt3a is essential for hematopoietic stem cell differentiation. *Nat Genet*. 2011;44(1):23-31.
20. Nam AS, Dusaj N, Izzo F, et al. Single-cell multi-omics of human clonal hematopoiesis reveals that DNMT3A R882 mutations perturb early progenitor states through selective hypomethylation. *Nat Genet*. 2022;54(10):1514-1526.
21. Jeong M, Park HJ, Celik H, et al. Loss of Dnmt3a immortalizes hematopoietic stem cells in vivo. *Cell Rep*. 2018;23(1):1-10.
22. Jeong M, Sun D, Luo M, et al. Large conserved domains of low DNA methylation maintained by Dnmt3a. *Nat Genet*. 2014;46(1):17-23.
23. Hormaechea-Agulla D, Matatall KA, Le DT, et al. Chronic infection drives Dnmt3a-loss-of-function clonal hematopoiesis via IFNγ signaling. *Cell Stem Cell*. 2021;28(8):1428-1442.e6.
24. Zioni N, Bercovich AA, Chapal-Ilani N, et al. Inflammatory signals from fatty bone marrow support DNMT3A driven clonal hematopoiesis. *Nat Commun*. 2023;14(1):2070.
25. Jaiswal S, Fontanillas P, Flannick J, et al. Age-related clonal hematopoiesis associated with adverse outcomes. *N Engl J Med*. 2014;371(26):2488-2498.
26. Genovese G, Kähler AK, Handsaker RE, et al. Clonal hematopoiesis and blood-cancer risk inferred from blood DNA sequence. *N Engl J Med*. 2014;371(26):2477-2487.
27. Coombs CC, Zehir A, Devlin SM, et al. Therapy-related clonal hematopoiesis in patients with non-hematologic cancers is common and associated with adverse clinical outcomes. *Cell Stem Cell*. 2017;21(3):374-382.e4.
28. Bhattacharya R, Zekavat SM, Haessler J, et al. Clonal hematopoiesis is associated with higher risk of stroke. *Stroke*. 2022;53(3):788-797.
29. Bolton KL, Koh Y, Foote MB, et al. Clonal hematopoiesis is associated with risk of severe Covid-19. *Nat Commun*. 2021;12(1):5975.
30. Hecker JS, Hartmann L, Rivière J, et al. CHIP and hips: clonal hematopoiesis is common in patients undergoing hip arthroplasty and is associated with autoimmune disease. *Blood*. 2021;138(18):1727-1732.
31. Fabre MA, de Almeida JG, Fiorillo E, et al. The longitudinal dynamics and natural history of clonal haematopoiesis. *Nature*. 2022;606(7913):335-342.
32. Uddin MDM, Nguyen NQH, Yu B, et al. Clonal hematopoiesis of indeterminate potential, DNA methylation, and risk for coronary artery disease. *Nat Commun*. 2022;13(1):5350.
33. Schiroli G, Kartha V, Duarte FM, et al. Cell of origin epigenetic priming determines susceptibility to Tet2 mutation. *Nat Commun*. 2024;15(1):4325.
34. Tovy A, Rosas C, Gaikwad AS, et al. Perturbed hematopoiesis in individuals with germline DNMT3A overgrowth Tatton-Brown-Rahman syndrome. *Haematologica*. 2022;107(4):887-898.
35. Barrachina MN, Pernes G, Becker IC, et al. Efficient megakaryopoiesis and platelet production require phospholipid remodeling and PUFA uptake through CD36. *Nat Cardiovasc Res*. 2023;2(8):746-763.
36. Courson JA, Lam FW, Langlois KW, Rumbaut RE. Histone-stimulated platelet adhesion to mouse cremaster venules in vivo is dependent on von Willebrand factor. *Microcirculation*. 2022;29(8):e12782.
37. Stark RJ, Aghakasiri N, Rumbaut RE. Platelet-derived toll-like receptor 4 (Tlr-4) is sufficient to promote microvascular thrombosis in endotoxemia. *PLoS One*. 2012;7(7):e41254.
38. Williamson MR, Dietrich K, Hackett MJ, et al. Rehabilitation augments hematoma clearance and attenuates oxidative injury and ion dyshomeostasis after brain hemorrhage. *Stroke*. 2017;48(1):195-203.
39. Pietras EM, Reynaud D, Kang YA, et al. Functionally distinct subsets of lineage-biased multipotent progenitors control blood production in normal and regenerative conditions. *Cell Stem Cell*. 2015;17(1):35-46.
40. Reyes JM, Tovy A, Zhang L, et al. Hematologic DNMT3A reduction and high-fat diet synergize to promote weight gain and tissue inflammation. *iScience*. 2024;27(3):109122.
41. Christodoulou C, Spencer JA, Yeh SCA, et al. Live-animal imaging of native haematopoietic stem and progenitor cells. *Nature*. 2020;578(7794):278-283.
42. Ramabadran R, Wang JH, Reyes JM, et al. DNMT3A-coordinated splicing governs the stem state switch towards differentiation in embryonic and haematopoietic stem cells. *Nat Cell Biol*. 2023;25(4):528-539.
43. Carrelha J, Mazzi S, Winroth A, et al. Alternative platelet differentiation pathways initiated by nonhierarchically related hematopoietic stem cells. *Nat Immunol*. 2024;25(6):1007-1019.

44. Schmitt A, Guichard J, Massé JM, Debili N, Cramer EM. Of mice and men: comparison of the ultrastructure of megakaryocytes and platelets. *Exp Hematol*. 2001;29(11):1295-1302.

45. Mohammed BM, Monroe DM, Gailani D. Mouse models of hemostasis. *Platelets*. 2020;31(4):417-422.

46. Heuston EF, Keller CA, Lichtenberg J, et al. Establishment of regulatory elements during erythro-megakaryopoiesis identifies hematopoietic lineage-commitment points. *Epigenetics Chromatin*. 2018;11(1):22.

47. Boyer SW, Schroeder AV, Smith-Berdan S, Forsberg EC. All hematopoietic cells develop from hematopoietic stem cells through Flk2/Flt3-positive progenitor cells. *Cell Stem Cell*. 2011;9(1):64-73.

48. Nangalia J, Nice FL, Wedge DC, et al. DNMT3A mutations occur early or late in patients with myeloproliferative neoplasms and mutation order influences phenotype. *Haematologica*. 2015;100(11):e438-e442.

49. O'Sullivan JM, Mead AJ, Psaila B. Single-cell methods in myeloproliferative neoplasms: old questions, new technologies. *Blood*. 2023;141(4):380-390.